

Article

# Investigation of Inverted Perovskite Solar Cells for Viscosity of PEDOT:PSS Solution

Pao-Hsun Huang<sup>1</sup>, Yeong-Her Wang<sup>1</sup>, Chien-Wu Huang<sup>2</sup>, Wen-Ray Chen<sup>3</sup>  
and Chien-Jung Huang<sup>2,\*</sup>

<sup>1</sup> Institute of Microelectronics, Department of Electrical Engineering, National Cheng Kung University, Tainan 70101, Taiwan; mdi12345paul@gmail.com (P.-H.H.); yhw@ee.ncku.edu.tw (Y.-H.W.)

<sup>2</sup> Department of Applied Physics, National University of Kaohsiung, Nanzih, Kaohsiung 81148, Taiwan; go40120@gmail.com

<sup>3</sup> Department of Electronic Engineering, National Formosa University, Yunlin 632, Taiwan; chenwr@nfu.edu.tw

\* Correspondence: chien@nuk.edu.tw; Tel.: +886-7-5919475; Fax: +886-5919357

Received: 31 July 2018; Accepted: 28 August 2018; Published: 6 September 2018



**Abstract:** In this paper, we demonstrate that the inverted  $\text{CH}_3\text{NH}_3\text{PbI}_3$  (perovskite) solar cells (PSCs) based on fullerene ( $\text{C}_{60}$ ) as an acceptor is fabricated by applying an improved poly(3,4-ethylenedioxythiophene):poly(styrenesulfonate) (PEDOT:PSS) solution as a hole transport layer (HTL). The power conversion efficiency (PCE) of inverted PSCs is increased by 37.5% with stable values of open-circuit voltage ( $V_{\text{OC}}$ ) and fill factor (FF) because we enhance the viscosity of the PEDOT:PSS solution, indicating the perfect effect on both external quantum efficiency (EQE) and surface grain size. The characteristics of the PEDOT:PSS solution, which is being improved through facile methods of obtaining excellent growth of PEDOT:PSS thin film, have a considerable impact on carrier transport. A series of further processing fabrications, including reliable and feasible heating and stirring techniques before the formation of the PEDOT:PSS thin film via spin-coating, not only evaporate the excess moisture but also obviously increase the conductivity. The raised collection of holes become the reason for the enhanced PCE of 3.0%—therefore, the stable performance of FF and  $V_{\text{OC}}$  are attributed to lower series resistance of devices and the high-quality film crystallization of perovskite and organic acceptors, respectively.

**Keywords:** perovskite; PEDOT:PSS solution; heating and stirring; solar cells

## 1. Introduction

One of the most important forms of renewable energy in the past decade has been solar energy. In particular, solar cells based on hybrid organic–inorganic perovskite structures have developed rapidly due to outstanding breakthroughs in the milestone of higher power conversion efficiency (PCE), which has been researched and published from 3.8% to 22.7% over the past few years [1–7]. Perovskite solar cells (PSCs) have been regarded as a promising next-generation optoelectronic device according to a series number of remarkable properties, including superior optical and electrical ability, simple solution processing, and low-cost fabrication [1,2,8–10]. In addition, the organ-metallic halide perovskite is suitable for many organic solvents, engineering with excellent solubility via fabricating various volume ratios, including dimethyl sulfoxide (DMSO), *N,N*-Methylformamide (DMF), and  $\gamma$ -butyrolacton (GBL), etc. [11–13]. Moreover, the perovskite light-emitting diodes (PeLEDs) have also improved in external quantum efficiency (EQE) values, such as for green emission of 9.3% and near-infrared emission of 11.7% [8,14].

To date, the structure of PSCs have been classified into conventional and inverted categories. Conventional PSCs generally obtain a high PCE but are not suitable for flexible future devices.

Conventional PSCs contain a metal oxide as an electron transport layer (ETL), which is rigid and requires high temperature processing for perfect electrical properties [15–19]. On the other hand, inverted PSCs have a planar structure such as the following: glass substrate/indium tin oxide (ITO)/poly(3,4-ethylenedioxythiophene):poly(styrenesulfonate) (PEDOT:PSS) as a hole transport layer, (HTL)/perovskite/fullerene (C<sub>60</sub>)/bathocuproine (BCP)/silver (Ag). It can be fabricated by simple and low-temperature processing methods used in our previous research [13,20–22]. In general, the performance of PSCs mainly relies on the quality of the perovskite film composited of methylammonium lead halide (CH<sub>3</sub>NH<sub>3</sub>PbI<sub>3</sub>, MAI), particularly in the inverted structure, which does not have a mesoscopic structure to control crystal growth in the film [3,7–9,13,15–17,23].

The PEDOT:PSS material is typically utilized as an HTL in organic and perovskite optoelectronic devices as a solution for disadvantages in optical and electrical properties [11,24–26]. PEDOT:PSS is considered to be a promising candidate due to its high flexibility, reasonably low material cost, and ability to be deposited using a wide variety of coating processes. Its conductivity ranges between an order of 1 and 10<sup>−5</sup> S × cm<sup>−1</sup>, depending on the ratio of PEDOT to PSS [25]. PEDOT:PSS has good mechanical properties that are largely dependent on the amount of moisture available in its environment. Although many metal oxides, such as molybdenum trioxide (MoO<sub>3</sub>) and tungsten trioxide (WO<sub>3</sub>) are conventionally used as an HTL due to their excellent ease of deposition as a thin film, both transmit at a visible wavelength range and surface roughness between HTL and the active layer of the metal oxide films which are not perfect and suitable for inverted PSCs [3,5,7,13,20,21]. Recently, the conductivity and transparency of the PEDOT:PSS film has been highly enhanced and extended to 4000 S/cm by various treatment processes and 97% at the visible range, respectively. In other words, the PEDOT:PSS layer not only reduces the energy barrier between the highest occupied molecular orbital (HOMO) of the active layer, but also improves the work function of the ITO electrode to fluently transport the hole charge. The surface of the ITO also smoothens after spin-coating the PEDOT:PSS solution, leading to favorable growth of the perovskite layer. The work function of PEDOT:PSS can be tuned to better align with the valence band of the perovskite film [26], thereby improving the holes collection and consequently enhancing device performance. In order to improve the performance of inverted PSCs using PEDOT:PSS, the optimization of HTL is important. Thus, a series of engineering improvements, including for the thin film, solution, and solvent, have been explored and investigated to try and decrease costs during each fabrication process.

The advantages of spin-coating are the simplicity and relative ease with which they can be set up, coupled with the thin and uniform coating that can be achieved. Because of the ability to have high spin speeds, the high airflow leads to fast drying times, which in turn results in high consistency at both macroscopic and nano-length scales. Although the PCE of the standard inverted PSCs using PEDOT:PSS is about 13% while PCE above 16% has been achieved with additives and modifications to the PEDOT:PSS layer [5,26], the cost they consume as a whole does not match the principle of economic efficiency. In this paper, we report a reliable and feasible method to improve the characteristics of PEDOT:PSS and further increase the performance of inverted PSCs via spin-coated PEDOT:PSS film as HTL. The optimized fullerene-based PSCs show a significantly enhanced PCE of 11% because of different concentrations of diluted PEDOT:PSS solution via heating and stirring in the preparation of the PEDOT:PSS solution.

## 2. Materials and Methods

### 2.1. Preparation of the PEDOT:PSS Solution

We took different amounts of poly(3,4-ethylenedioxythiophene):poly(styrenesulfonate) (PEDOT:PSS) solution for processing—1700, 1500, and 1300 μL (1.3–1.7 wt % from H. C. Starck Baytron P AI-4083, purchased from Heraeus Co., Hanau, Germany). Each PEDOT:PSS solution was firstly filtered with a polytetrafluoroethylene (PTFE) filter of pore size 0.45 before being stably stirred at 300 rpm at 90 °C for 20 min on a hotplate to further remove excess moisture and promote the quality of each PEDOT:PSS

solution. At the same time, we sealed the beaker with dustless paper to absorb the water vapor from the heating process. The temperature value was obtained from the reading on the hotplate instrument.

## 2.2. Fabrication of the PEDOT:PSS Thin Film

The glass substrate-coated indium tin oxide (ITO) (AimCore Technology, Hsinchu, Taiwan) with a sheet resistance ( $R_s$ ) of  $7 \Omega/\text{sq}$  was firstly patterned and sequentially cleaned by performing consecutive and ultrasonic treatment in acetone, methanol, and deionized water for 5 min each. Moreover, pre-cleaned ITO-glass substrate was dried under a nitrogen blow. The oxygen ( $\text{O}_2$ ) plasma treatment on the ITO-glass substrate was conducted using radio frequency (RF) power at 10 W for 2 min at a pressure of 0.45 torr to enhance the work function [26–28]. The prepared PEDOT:PSS solution was spin-coated onto the prepared ITO-glass substrate following the two-step parameters process (1500 rpm for 5 s for the first step, and 5000 rpm for 30 s for the second), and was annealed at  $120^\circ\text{C}$  for 15 min afterwards to fabricate HTL.

## 2.3. Preparation and Fabrication of $\text{CH}_3\text{NH}_3\text{PbI}_3$ Precursor Solution

The  $\text{CH}_3\text{NH}_3\text{I}$  of 1.25 M (>98%, Dyesol, Queanbeyan, Australia) and  $\text{PbI}_2$  of 1.25 M (99.99%, Alfa Aesar, Haverhill, MA, USA) were dissolved in the allocated solvent of 1 mL, in which the volume ratio ( $v/v$ ) of dimethyl sulfoxide (DMSO) to  $\gamma$ -butyrolacton (GBL) was mixed 1:1, to prepare the  $\text{CH}_3\text{NH}_3\text{PbI}_3$  (perovskite) precursor solutions. Then, the perovskite precursor solution was stirred for 24 h and filtered with the PTFE filter of pore size 0.45 to fabricate the perovskite layer, which was deposited by using the solvent engineering technique [11,12,22,27].

## 2.4. Fabrication and Characteristics of Perovskite Solar Cells

Figure 1a presents the configuration of the inverted perovskite solar cells (PSCs) as glass substrate/indium tin oxide (ITO)/PEDOT:PSS/perovskite/fullerene ( $\text{C}_{60}$ )/bathocuproine (BCP)/silver (Ag). At the same time, the relative energy level of PSCs presents directly how the electron and hole move to anode and cathode in Figure 1b. The fabrication of HTL (PEDOT:PSS) was as the above statement (2.2) and the substrate was then transferred into a glove box filled with pure  $\text{N}_2$ . Next, the perovskite precursor solution was spin-coated onto the PEDOT:PSS layer via the consecutive two-step method at 1000 rpm and 5000 rpm for 10 s and 20 s, respectively, to form a perovskite layer [11]. During the spin-coating process at 5000 rpm, the toluene solution of 150  $\mu\text{L}$  was dripped onto the wet and spinning film and annealed on a hotplate at  $90^\circ\text{C}$  for 15 min afterwards. The organic materials of  $\text{C}_{60}$  and BCP were used as an electron acceptor and an ETL, respectively. The organic materials and Ag were deposited via vacuum thermal evaporation under a pressure of  $4.8 \times 10^{-6}$  torr. The deposited rate of organic materials was approximately between 0.02 nm/s and 0.04 nm/s, and the Ag was deposited through a particular shadow mask, yielding an active area of 0.2  $\text{cm}^2$  at a deposition rate of 0.1 nm/s. The deposited rate and film thicknesses were monitored using a quartz crystal oscillator. There were at least 12 samples per type, which allowed for the simultaneous comparison of the reproducibility and stability of the photoelectric properties. In addition, we designed each batch of experimental processes to successfully set up four devices that could operate independently of each other.

The current density-voltage (J–V) characteristics of PSCs were measured using a power source meter (Keithley 2400, Keithley, Cleveland, AL, USA) under an illumination of  $100 \text{ mW}/\text{cm}^2$  produced by an AM1.5G sun simulator (Oriel 96,000 150 W Xe lamp, Newport, Taipei, Taiwan). The light intensity was calibrated using a reference solar cell and meter (Oriel 91150, Newport, Taipei, Taiwan). All the devices were encapsulated, and the active area was masked with a metal mask (area of  $6 \text{ mm}^2$ ) before the measurement of J–V characteristics was executed to ensure the reliability and accuracy of parameters. However, the scanning speed of the voltage was 0.02 V/s and the direction of scanning was from the negative voltage (–1 V) to the positive voltage (+1 V) in the measurement of J–V characteristics. For the atomic force microscope (AFM) measurement (XE-70, Park Systems, Suwon, Korea), the surface morphologies were determined in noncontact mode in air. The absorption spectra

of the films were measured using a UV–vis–NIR spectrophotometer (UV-3900, Hitachi, Tokyo, Japan) in the 400–850 nm wavelength range. The external quantum efficiency (EQE) measurements were performed using the Solar Cell QE/IPCE measurement system (QE-3000, Titan Electro-Optics, Taipei, Taiwan). The EQE spectra were performed with a SR830 lock-in amplifier (Stanford Research System, Titan Electro-Optics, Taipei, Taiwan) under monochromatic illumination at a chopping frequency of 185 Hz. The X-ray diffraction (XRD) data were measured by an Ultima IV X-ray diffractometer (Rigaku, Tokyo, Japan).

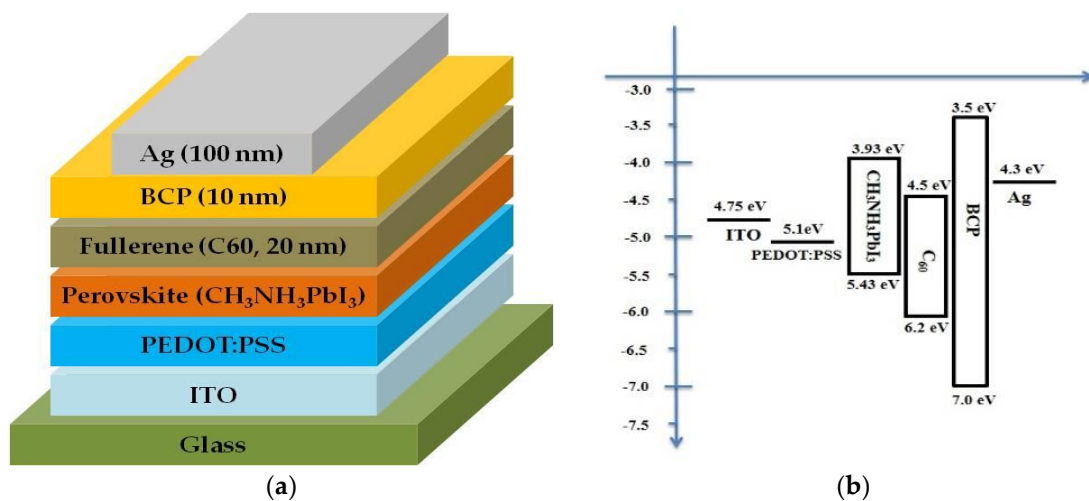


**Figure 1.** The (a) structure and (b) energy level of each material used for perovskite solar cells (PSCs) in this study.

### 3. Results

The  $\text{CH}_3\text{NH}_3\text{PbI}_3$  (perovskite) solar cells (PSCs) had been accomplished by inverted structure and three improved poly(3,4-ethylenedioxythiophene):poly(styrenesulfonate) (PEDOT:PSS) thin films in the Figure 2a, which were controlled under three extractions of 1700, 1500, and 1300  $\mu\text{L}$  strictly. Both current density-voltage (J–V) curves and external quantum efficiency (EQE) results of the inverted PSCs, fabricated with 100 nm cathode (silver, Ag), are shown, respectively, in Figure 2 to intuitively showcase the device performance. After the program calculation, the maximum rectangular area under the J–V curve can be preliminarily determined regarding which device has excellent performance (red curve), indicating the higher PCE. It is also obviously found that the inverted PSC with an extraction of 1500  $\mu\text{L}$  attained the largest area, going upward slowly and smoothly as the voltage rises steadily, as an alternative to other devices in Figure 2a. In Figure 2b, the trend of EQE spectra regarding inverted PSCs with an extraction of 1500  $\mu\text{L}$  has the same performance as that of an extraction level of 1700  $\mu\text{L}$  between 300 and 420 nm, which is higher than that of the lowest extraction level of 1300  $\mu\text{L}$ . From 420 to 800 nm of EQE spectra, however, the light transformation for the electron is much better than that of inverted PSCs with an extraction level of 1300 and 1700  $\mu\text{L}$ , by integrating the area under the EQE curve. Therefore, the superb performance and most effective photoelectron conversion efficiency can be accomplished and obtained respectively from the inverted PSCs with PEDOT:PSS extraction of 1500  $\mu\text{L}$  by the EQE spectra in Figure 2b.

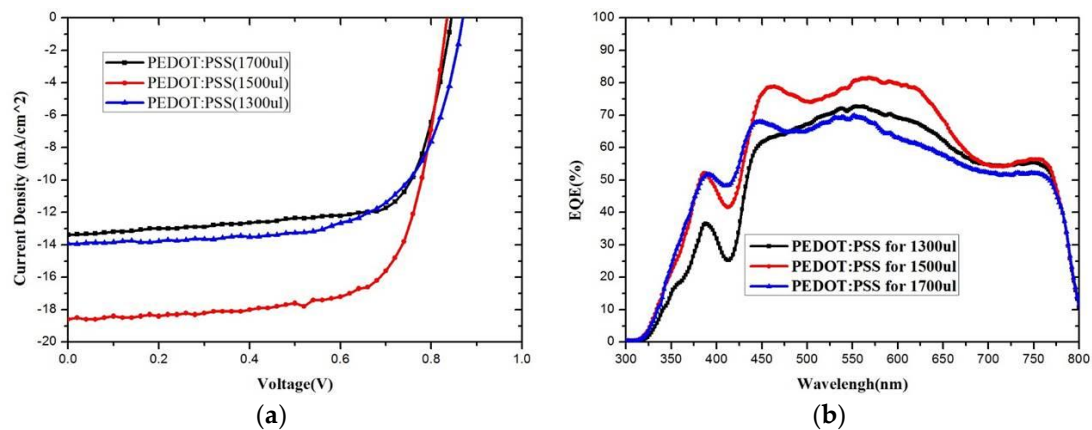


**Figure 2.** The (a) J–V curve and (b) external quantum efficiency (EQE) results for inverted PSCs, fabricated with 100 nm cathode and controlled under three extractions of 1700, 1500, and 1300  $\mu\text{L}$  strictly.

In order to explore each device performance in detail, Table 1 also presents the various parameters of photovoltaic performance for inverted PSCs with 100 nm Ag, including short-current density ( $J_{\text{SC}}$ ), open-circuit voltage ( $V_{\text{OC}}$ ), fill factor (FF), series resistance ( $R_{\text{S}}$ ), shunt resistance ( $R_{\text{sh}}$ ), and power conversion efficiency (PCE). The  $V_{\text{OC}}$  of all inverted PSCs is converging steadily on  $\sim 0.8$  V, and the inverted PSCs with an extraction of 1500  $\mu\text{L}$  performs better in  $J_{\text{SC}}$ , FF, PCE, and  $R_{\text{S}}$  for 17.39  $\text{mA}/\text{cm}^2$ , 0.64, 72.42  $\Omega \times \text{cm}^2$ , and 9.71%, respectively. At the same time, the PCE of the inverted PSCs with extraction levels of 1300 and 1700  $\mu\text{L}$  are 8.21 and 8.00% because of the lower  $J_{\text{SC}}$  of 13.38 and 13.91  $\text{mA}/\text{cm}^2$ , respectively. The FF can also directly decide the device performance. The lower value of  $R_{\text{S}}$  of 61.1  $\Omega \times \text{cm}^2$  is achieved by the inverted PSCs with an extraction of 1500  $\mu\text{L}$ , and the higher value of  $R_{\text{sh}}$  of 9760  $\Omega \times \text{cm}^2$  is accomplished by the inverted PSCs with an extraction of 1300  $\mu\text{L}$ . It also reflects the maximum values of  $J_{\text{SC}}$  and  $V_{\text{OC}}$ . However, the  $V_{\text{OC}}$  and FF of all inverted PSCs converge steadily on  $\sim 0.8$  V and 0.7, respectively. The device which has improved PEDOT:PSS with an extraction of 1500  $\mu\text{L}$  has a perfect PCE of 11.0%, which is the highest score out of all other devices. The maximum  $J_{\text{SC}}$  and  $R_{\text{sh}}$  are achieved at about 18.6  $\text{mA}/\text{cm}^2$  and 9760  $\Omega \times \text{cm}^2$ , respectively. In order to understand what changes have arisen from electron transport under the fabrication of three parameters, we measured the surface roughness via the AFM instrument.

**Table 1.** The photovoltaic performance of the inverted PSCs<sup>1</sup> fabricated using three extractions of PEDOT:PSS solution of 1700, 1500, and 1300  $\mu\text{L}$ , and the 100 nm Ag.

Extraction of PEDOT:PSS Solution ( $\mu\text{L}$ )	$J_{\text{sc}}$ ( $\text{mA}/\text{cm}^2$ )	$V_{\text{oc}}$ (V)	FF	$R_{\text{s}}$ ( $\Omega \times \text{cm}^2$ )	$R_{\text{sh}}$ ( $\Omega \times \text{cm}^2$ )	PCE (%)
1700	13.38 $\pm$ 0.14	0.85 $\pm$ 0.04	0.72 $\pm$ 0.12	79.0 $\pm$ 3.5	8074 $\pm$ 45	8.21 $\pm$ 0.12
1500	18.60 $\pm$ 0.09	0.84 $\pm$ 0.04	0.71 $\pm$ 0.14	61.1 $\pm$ 2.6	9760 $\pm$ 37	11.00 $\pm$ 0.07
1300	13.91 $\pm$ 0.15	0.87 $\pm$ 0.02	0.66 $\pm$ 0.13	72.3 $\pm$ 4.2	9049 $\pm$ 28	8.00 $\pm$ 0.12

<sup>1</sup> The structure of PSCs: Glass/ITO/PEDOT:PSS/Perovskite/ $\text{C}_{60}$ /BCP/Ag (100 nm).

Figure 3 shows the surface morphologies and microscope images of each improved PEDOT:PSS of 1700, 1500, and 1300  $\mu\text{L}$ . From the microscope images of improved PEDOT:PSS of 1700 and 1300  $\mu\text{L}$ , can be directly seen that the difference between the highest and lowest point is immense through the color difference in Figure 3a,c. However, Figure 3b shows a surface morphology with an island shape with a lesser difference in color. Table 2 also explores in detail the surface roughness values of 1.19, 1.513, and 1.502 nm for each improved PEDOT:PSS of 1700, 1500, and 1300  $\mu\text{L}$ , respectively. These results explain why the PCE of the device with an extraction level of 1500  $\mu\text{L}$  is relatively higher than other devices. Further AFM measurement results with detailed measure parameters have been added in the Figure S2a–c.

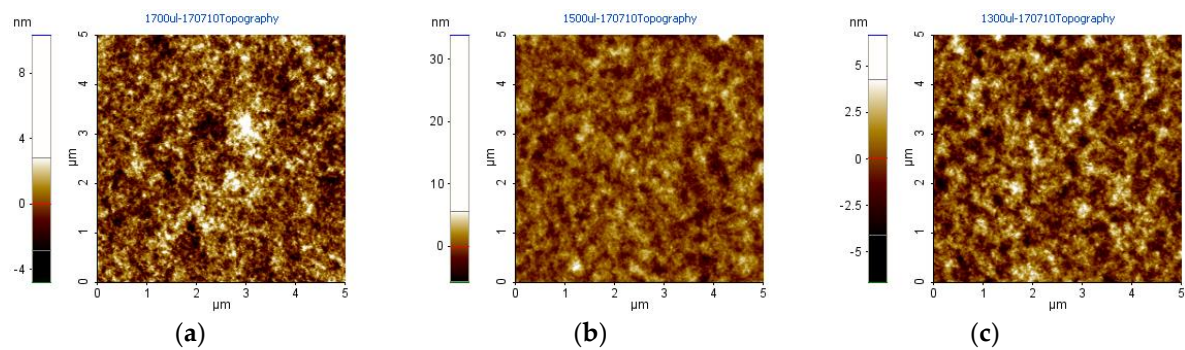


**Figure 3.** The surface roughness and grain size of improved PEDOT:PSS with three extractions of (a) 1700, (b) 1500, and (c) 1300  $\mu\text{L}$  from an atomic force microscope (AFM) measurement.

**Table 2.** The surface roughness ( $R_q$ ) values about improved PEDOT:PSS with three extractions of 1700, 1500, and 1300  $\mu\text{L}$ , which were coated on the glass substrate.

Extraction of PEDOT:PSS Solution ( $\mu\text{L}$ )	$R_q$ (nm)
1700	1.190
1500	1.513
1300	1.502

#### 4. Discussion

The growth of  $\text{CH}_3\text{NH}_3\text{PbI}_3$  (perovskite) thin film depend on the surface morphologies of poly(3,4-ethylenedioxythiophene):poly(styrenesulfonate) (PEDOT:PSS) thin film. That is to say, one of the most important factors for high power conversion efficiency (PCE) in inverted PSCs is the quality of the growth of perovskite thin film, which is deposited on a PEDOT:PSS thin film. The absorption spectrum of perovskite and fullerene ( $\text{C}_{60}$ ) material, which is an active layer in the inverted PSCs, is also presented from 400–850 nm in the Figure S1. The wavelength range of light absorption is roughly concentrated from 400–650 nm, which corresponds to the result of EQE measurement in Figure 2b. Therefore, it is found that the short-current density ( $J_{\text{SC}}$ ) of inverted PSCs, which is fabricated by improved PEDOT:PSS solution, is improved respectively from 13.38 to 18.60  $\text{mA}/\text{cm}^2$  in Table 1. On the other hand, the fill factor (FF) and open-circuit voltage ( $V_{\text{OC}}$ ) are also maintained stably at  $\sim 0.70$  and 0.80 V. Further improvements can be seen from the external quantum efficiency (EQE) results in Figures 2b and 3b. The EQE can be interpreted as the following equation [13,15]:

$$\eta_{\text{EQE}} = \eta_{\text{A}} \times \eta_{\text{ED}} \times \eta_{\text{CT}} \times \eta_{\text{CC}} \quad (1)$$

where  $\eta_{\text{A}}$  is the absorption efficiency of incident photons,  $\eta_{\text{ED}}$  is the efficiency of photo-generated excitons that diffuse to the heterojunction interface,  $\eta_{\text{CT}}$  is the charge transfer efficiency, and  $\eta_{\text{CC}}$  is the charge collection efficiency. In this great performance of  $J_{\text{SC}}$ , the EQE spectrum of the devices is associated with the  $\eta_{\text{A}}$  and  $\eta_{\text{CT}}$ . According to the area integration of the EQE curve from 300 to 800 nm, the  $\eta_{\text{CT}}$  presents the amount of photos converted to electrons and explains why the enhancement of  $J_{\text{SC}}$  has as a percentage of 26.375% under the average condition.

At the same time, the steady  $V_{\text{OC}}$  of  $\sim 0.8$  V and low series resistance ( $R_{\text{S}}$ ) of  $61.1 \Omega \times \text{cm}^2$  are the second factor for the enhanced PCE from 8.00 to 11.00%. In Figure 1b, it is clear that the  $V_{\text{OC}}$ , which is associated with the energy level difference between the highest occupied molecular orbital of the donor ( $\text{HOMO}_{\text{D}}$ ) and the lowest unoccupied molecular orbital of the acceptor ( $\text{LUMO}_{\text{A}}$ ), can be sustained at a steady state because the donor and acceptor materials have not been changed. More detailed information about  $V_{\text{OC}}$  is related to the following equation:

$$V_{OC} = \frac{1}{e}(LUMO_A - HOMO_D - \Delta) - \frac{KT}{e} \ln\left(\frac{n_e n_h}{N_c^2}\right) \quad (2)$$

where  $n_e$  and  $n_h$  are the electron and hole densities in the  $C_{60}$  and the donor at open circuit,  $K$  is the Boltzmann constant,  $\Delta$  is the energy shift,  $T$  is the Kelvin scale, and  $N_c$  is the density of conduction states at the band edge of  $C_{60}$  and donor (assumed to be equal here). The commonly accepted value,  $V_{OC} = (LUMO_A - HOMO_D)$ , is obtained from the above equation only at  $T = 0$  K. The validity of the first term in the equation has been verified for a number of 0.3 V of previously unknown origin [20–22]. At finite  $T$ , because of the fundamental statistics of Fermions, the quasi-Fermi levels move away from  $LUMO_A$  and  $HOMO_D$ , respectively, and into the gap above the polymer HOMO energy level and LUMO energy level. The resulting reduction in  $V_{OC}$  is given by the second term in the equation and is the origin of the “missing 0.3 V” [29]. In general, the  $R_s$  of the device would also present an upward trend when the thickness of the electrode (anode and cathode) increases gradually. But the thickness of the whole device should also be carefully considered, which reflects on the value of FF. To characterize a solar cell, three important parameters are usually considered;  $V_{OC}$ ,  $J_{SC}$ , and FF [29–31]. The FF not only depends on the recombination and extraction of free charges, but also gives insight into why the FF changes so much with light intensity, thickness, and material properties in the bulk-heterojunction solar cells. The definition of FF can be expressed as the following equation:

$$FF = \frac{J_{MPP} V_{MPP}}{J_{SC} V_{OC}} \quad (3)$$

where the  $J_{MPP}$  and  $V_{MPP}$  are the current density and voltage at the maximum power point (MPP), respectively. It is amazing that the magnitude of the increase has been expressed remarkably as a percentage of 37.5% in PCE when the  $V_{OC}$  value is at a steady state of  $\sim 0.8$  V.

The interface engineering between the active layer and electrode is gradually an immense issue of PSCs. Both the hole transport layer (HTL) and electron transport layer (ETL) play an unyielding role in effectively transporting electrons and holes. Thus, we can clearly find and compare that the inverted PSCs with an improved PEDOT:PSS thin film of 1500  $\mu$ L extraction has a greater grain size than that of another devices shown in Figure 3b. The collection of holes is affected by the grain size of PEDOT:PSS thin film, although the surface roughness ( $R_q$ ) is close for each device in Table 2. The surface morphology of PEDOT:PSS thin film has a clear island shape in Figure 3b, leading to the rise in  $J_{SC}$ . The purpose of optimizing the viscosity or concentration of the PEDOT:PSS solution via removing excess water is to fabricate the superb thin film. The evaporation of excess moisture in the PEDOT:PSS solution, which was treated through the hotplate before the fabrication of HTL, is the main reason for the PCE increase of about 2.0%. We used a sophisticated electronic balance to measure the total weight before heating as well as the weight loss from the evaporated moisture after heating. The weight of the total PEDOT:PSS solution and evaporated moisture were about 22.8337 g and 0.4812 g. The viscosity of the PEDOT:PSS solution has been improved successfully by removing excess moisture to increase the conductivity of the PEDOT:PSS solution. On the other hand, we also found that the optimized PEDOT:PSS thin film will make the growth of perovskite film more efficient after a series of solution preprocessing with heating and stirring. How the maximum values of FF and  $J_{SC}$  can be achieved under the condition of optimized  $R_s$  will be serious topics for study in the future. The thickness and characteristics of used materials, especially the HTL, ETL, and perovskite layer, will be key factors affecting the PCE of the PSCs. Non-fullerene and the cascade concept needs to be further investigated and applied to PSCs.

## 5. Conclusions

The inverted  $CH_3NH_3PbI_3$  (perovskite) solar cells (PSCs) with an optimized hole transport layer (HTL) and electrode thickness have been fabricated, and significant power conversion efficiency (PCE) has been accomplished from 8.00 to 11.0%. We found a significant increase in viscosity when excess

moisture was removed in the poly(3,4-ethylenedioxythiophene):poly(styrenesulfonate) (PEDOT:PSS) solution as an HTL through using an effective and simple method. Both the improved conductivity and surface morphology of the island shape from PEDOT:PSS helped the collection and transport of the hole. Besides, optimization of the viscosity or concentration of the PEDOT:PSS solution via removing excess water was in order to fabricate the superb thin film. The fabrication process, including the heating and stirring, was found to increase the viscosity and collection of electrons—however, the trend of series resistance ( $R_S$ ) decreased from 79.2 to 61.1  $\Omega \times \text{cm}^2$ . Three important parameters in the PSCs showed an abundant improvement—39.01% for short-current density ( $J_{SC}$ ) and 1.35 times for PCE, under a steady-state value of open-circuit voltage ( $V_{OC}$ ) of  $\sim 0.8$  V, and a fill factor (FF) of 0.70. Therefore, the stable performance of FF and  $V_{OC}$  are attributed respectively to a lower series resistance of the device and high-quality film crystallization of the perovskite and organic acceptor. Further investigation and improvement of the non-fullerene and cascade concept is expected by growing a water-resistive coating or ion doping onto each thin film in the future.

**Supplementary Materials:** The following are available online at <http://www.mdpi.com/2073-4352/8/9/358/s1>, Figure S1: The normalized absorbance spectrum of active layer, the perovskite material (red curve) and fullerene material ( $C_{60}$ , blue curve), in the inverted perovskite solar cells from 400–850 nm, Figure S2: The AFM measurement result for the PSCs with specific tilt angle (X-Y-Z of  $-40^\circ - 30^\circ - 30^\circ$ ) and scan area ( $5 \times 5 \mu\text{m}$ ), which is fabricated through improved PEDOT:PSS solution of: (a) 1700  $\mu\text{L}$ , (b) 1500  $\mu\text{L}$ , and (c) 1300  $\mu\text{L}$  as HTL.

**Author Contributions:** P.-H.H. and C.-W.H. analyzed the materials and designed the experiments; P.-H.H., Y.-H.W., C.-W.H., W.-R.C. and C.-J.H. performed the experiments and analyzed the results; Y.-H.W., C.-J.H. and W.-R.C. gave some useful information and suggestions for this work, and contributed the analysis tools; P.-H.H., Y.-H.W., C.-W.H., W.-R.C. and C.-J.H. discuss theories about the renewable energy named Perovskite solar cells. P.-H.H. and C.-W.H. drafted the manuscript and finalized the manuscript.

**Acknowledgments:** This work was partially supported by the Ministry of Science and Technology (MOST) of Taiwan under contract number: MOST 106-2221-E-390-016.

**Conflicts of Interest:** The authors declare no conflict of interest.

## References

1. Im, J.H.; Lee, C.R.; Lee, J.W.; Park, S.W.; Park, N.G. 6.5% efficient perovskite quantum-dot-sensitized solar cell. *Nanoscale* **2011**, *3*, 4088–4093. [[CrossRef](#)] [[PubMed](#)]
2. Burschka, J.; Pellet, N.; Moon, S.J.; Humphry-Baker, R.; Gao, P.; Nazeeruddin, M.K.; Grätzel, M. Sequential deposition as a route to high-performance perovskite-sensitized solar cells. *Nature* **2013**, *499*, 316–319. [[CrossRef](#)] [[PubMed](#)]
3. Liu, D.; Kelly, T.L. Perovskite solar cells with a planar heterojunction structure prepared using room-temperature solution processing techniques. *Nat. Photonics* **2014**, *8*, 133–138. [[CrossRef](#)]
4. Zhou, H.; Chen, Q.; Li, G.; Luo, S.; Song, T.B.; Duan, H.S.; Hong, Z.; You, J.; Liu, Y.; Yang, Y. Interface engineering of highly efficient perovskite solar cells. *Science* **2014**, *345*, 542–546. [[CrossRef](#)] [[PubMed](#)]
5. Popoola, I.K.; Gondal, M.A.; Qahtan, T.F. Recent progress in flexible perovskite solar cells: Materials, mechanical tolerance and stability. *Renew. Sustain. Energy Rev.* **2018**, *82*, 3127–3151. [[CrossRef](#)]
6. You, J.; Hong, Z.; Yang, Y.; Chen, Q.; Cai, M.; Song, T.B.; Chen, C.C.; Lu, S.; Liu, Y.; Zhou, H.; Yang, Y. Low-Temperature Solution-Processed Perovskite Solar Cells with High Efficiency and Flexibility. *ACS Nano* **2014**, *8*, 1674–1680. [[CrossRef](#)] [[PubMed](#)]
7. Ahn, N.; Son, D.Y.; Jang, I.H.; Kang, S.M.; Choi, M.; Park, N.G. Highly Reproducible Perovskite Solar Cells with Average Efficiency of 18.3% and Best Efficiency of 19.7% Fabricated via Lewis Base Adduct of Lead(II) Iodide. *J. Am. Chem. Soc.* **2015**, *137*, 8696–8699. [[CrossRef](#)] [[PubMed](#)]
8. Kojima, A.; Teshima, K.; Shirai, Y.; Miyasaka, T. Organometal Halide Perovskites as Visible-Light Sensitizers for Photovoltaic Cells. *J. Am. Chem. Soc.* **2009**, *131*, 6050–6051. [[CrossRef](#)] [[PubMed](#)]
9. Etgar, L.; Gao, P.; Xue, Z.; Peng, Q.; Chandiran, A.K.; Liu, B.; Nazeeruddin, M.K.; Grätzel, M. Mesoscopic  $\text{CH}_3\text{NH}_3\text{PbI}_3/\text{TiO}_2$  Heterojunction Solar Cells. *J. Am. Chem. Soc.* **2012**, *134*, 17396–17399. [[CrossRef](#)] [[PubMed](#)]
10. Lee, M.M.; Teuscher, J.; Miyasaka, T.; Murakami, T.N.; Snaith, H.J. Efficient Hybrid Solar Cells Based on Meso-Superstructured Organometal Halide Perovskites. *Science* **2012**, *338*, 643. [[CrossRef](#)] [[PubMed](#)]

11. Jeon, N.J.; Noh, J.H.; Kim, Y.C.; Yang, W.S.; Ryu, S.; Seok, S.I. Solvent engineering for high-performance inorganic–organic hybrid perovskite solar cells. *Nat. Mater.* **2014**, *13*, 897–903. [[CrossRef](#)] [[PubMed](#)]
12. Liu, Z.; Lee, E.C. Solvent engineering of the electron transport layer using 1,8-diiodooctane for improving the performance of perovskite solar cells. *Org. Electron.* **2015**, *24*, 101–105. [[CrossRef](#)]
13. Huang, P.H.; Wang, Y.H.; Ke, J.C.; Huang, C.J. The Effect of Solvents on the Performance of CH<sub>3</sub>NH<sub>3</sub>PbI<sub>3</sub> Perovskite Solar Cells. *Energies* **2017**, *10*, 599. [[CrossRef](#)]
14. Veldhuis, S.A.; Boix, P.P.; Yantara, N.; Li, M.; Sum, T.C.; Mathews, N.; Mhaisalkar, S.G. Perovskite Materials for Light-Emitting Diodes and Lasers. *Adv. Mater.* **2016**, *28*, 6804–6834. [[CrossRef](#)] [[PubMed](#)]
15. Rand, B.P.; Burk, D.P.; Forrest, S.R. Offset energies at organic semiconductor heterojunctions and their influence on the open-circuit voltage of thin-film solar cells. *Phys. Rev. B* **2007**, *75*, 115327. [[CrossRef](#)]
16. Jeng, J.Y.; Chen, K.C.; Chiang, T.Y.; Lin, P.Y.; Tsai, T.D.; Chang, Y.C.; Guo, T.F.; Chen, P.; Wen, T.C.; Hsu, Y.J. Nickel Oxide Electrode Interlayer in CH<sub>3</sub>NH<sub>3</sub>PbI<sub>3</sub> Perovskite/PCBM Planar-Heterojunction Hybrid Solar Cells. *Adv. Mater.* **2014**, *26*, 4107–4113. [[CrossRef](#)] [[PubMed](#)]
17. Ke, W.; Fang, G.; Wang, J.; Qin, P.; Tao, H.; Lei, H.; Liu, Q.; Dai, X.; Zhao, X. Perovskite Solar Cell with an Efficient TiO<sub>2</sub> Compact Film. *ACS Appl. Mater. Interfaces* **2014**, *6*, 15959–15965. [[CrossRef](#)] [[PubMed](#)]
18. Ma, Y.; Zheng, L.; Chung, Y.H.; Chu, S.; Xiao, L.; Chen, Z.; Wang, S.; Qu, B.; Gong, Q.; Wu, Z.; et al. A highly efficient mesoscopic solar cell based on CH<sub>3</sub>NH<sub>3</sub>PbI<sub>3</sub>Cl<sub>x</sub> fabricated via sequential solution deposition. *Chem. Commun.* **2014**, *50*, 12458–12461. [[CrossRef](#)] [[PubMed](#)]
19. Wu, Y.; Islam, A.; Yang, X.; Qin, C.; Liu, J.; Zhang, K.; Peng, W.; Han, L. Retarding the crystallization of PbI<sub>2</sub> for highly reproducible planar-structured perovskite solar cells via sequential deposition. *Energy Environ. Sci.* **2014**, *7*, 2934–2938. [[CrossRef](#)]
20. Ke, J.C.; Wang, Y.H.; Chen, K.L.; Huang, P.H.; Huang, C.J. Study of Small Molecule Organic Solar Cells Performance Based on Boron Subphthalocyanine Chloride and C<sub>60</sub>. *Int. J. Photoenergy* **2013**, *2013*, 5. [[CrossRef](#)]
21. Huang, P.H.; Wang, Y.H.; Ke, J.C.; Huang, C.J. Investigation of Various Active Layers for Their Performance on Organic Solar Cells. *Materials* **2016**, *9*, 667. [[CrossRef](#)] [[PubMed](#)]
22. Ke, J.C.; Wang, Y.H.; Chen, K.L.; Huang, C.J. Effect of temperature annealing treatments and acceptors in CH<sub>3</sub>NH<sub>3</sub>PbI<sub>3</sub> perovskite solar cell fabrication. *J. Alloys Compd.* **2017**, *695*, 2453–2457. [[CrossRef](#)]
23. Zhao, Y.; Wei, J.; Li, H.; Yan, Y.; Zhou, W.; Yu, D.; Zhao, Q. A polymer scaffold for self-healing perovskite solar cells. *Nat. Commun.* **2016**, *7*, 10228. [[CrossRef](#)] [[PubMed](#)]
24. Zhou, J.; Anjum, D.H.; Chen, L.; Xu, X.; Ventura, I.A.; Jiang, L.; Lubineau, G. The temperature-dependent microstructure of PEDOT/PSS films: Insights from morphological, mechanical and electrical analyses. *J. Mater. Chem. C* **2014**, *2*, 9903–9910. [[CrossRef](#)]
25. Stöcker, T.; Köhler, A.; Moos, R. Why does the electrical conductivity in PEDOT:PSS decrease with PSS content? A study combining thermoelectric measurements with impedance spectroscopy. *J. Polym. Sci. Part B Polym. Phys.* **2012**, *50*, 976–983. [[CrossRef](#)]
26. Chang, S.H.; Lin, K.F.; Chiu, K.Y.; Tsai, C.L.; Cheng, H.M.; Yeh, S.C.; Wu, W.T.; Chen, W.N.; Chen, C.T.; Chen, S.H.; et al. Improving the efficiency of CH<sub>3</sub>NH<sub>3</sub>PbI<sub>3</sub> based photovoltaics by tuning the work function of the PEDOT:PSS hole transport layer. *Sol. Energy* **2015**, *122*, 892–899. [[CrossRef](#)]
27. Ke, J.C.; Wang, Y.H.; Chen, K.L.; Huang, C.J. Effect of organic solar cells using various power O<sub>2</sub> plasma treatments on the indium tin oxide substrate. *J. Colloid Interface Sci.* **2016**, *465*, 311–315. [[CrossRef](#)] [[PubMed](#)]
28. Ke, J.C.; Wang, Y.H.; Chen, K.L.; Huang, C.J. Effect of organic solar cells using various sheet resistances of indium tin oxide and different cathodes: Aluminum, silver. *Synth. Met.* **2015**, *201*, 25–29. [[CrossRef](#)]
29. Brabec, C.J.; Cravino, A.; Meissner, D.; Sariciftci, N.S.; Fromherz, T.; Rispen, M.T.; Sanchez, L.; Hummelen, J.C. Origin of the Open Circuit Voltage of Plastic Solar Cells. *Adv. Funct. Mater.* **2001**, *7*, 374–380. [[CrossRef](#)]
30. Qi, B.; Wang, J. Fill factor in organic solar cells. *Phys. Chem. Chem. Phys.* **2013**, *15*, 8972–8982. [[CrossRef](#)] [[PubMed](#)]
31. Trukhanov, V.A.; Bruevich, V.V.; Paraschuk, D.Y. Fill factor in organic solar cells can exceed the Shockley-Queisser limit. *Sci. Rep.* **2015**, *5*, 11478. [[CrossRef](#)] [[PubMed](#)]

